

Allocation of CaCO_3 Polymorphs in Biological Systems: A Confocal Raman-AFM Study

U. Schmidt¹*, S. Hild², and A. Ziegler³

¹WITec GmbH, Lise-Meitner-Strasse 6, 89081 Ulm, Germany,

²Institute of Polymer Science, Johannes Kepler University, Altenbergstr.69, A-4020 Linz, Germany

³Central Facility for Electron Microscopy, University of Ulm, Albert-Einstein-Allee 11, 89081 Ulm, Germany

* ute.schmidt@witec.de

Introduction

Biological composites have attracted increasing interest because of their outstanding properties and versatility. Crustaceans are interesting models for the study of these materials. They have a mineralized exoskeleton (cuticle) that provides support and protection. The structural organization of the cuticle is ubiquitous in arthropods: a hierarchically structured organic matrix composed of planes of parallel chitin-protein fibers that are stacked in a twisted plywood organization [1] associated with various amounts of minerals. The land-dwelling crustacean *Porcellioscaber* (*P. scaber*) is a well-established model organism for the study of the bio-mineralization processes [2, 3]. Its cuticle contains two types of calcium carbonates: calcite and amorphous calcium carbonate (ACC) [4, 5]. In addition the *P. scaber* develops

sternal calcium carbonate deposits [6] that are electron and x-ray amorphous [7, 8]. The presence of ACC is of particular interest because it plays an important role in the development of mineralized biological tissues. It is thought to be a precursor of crystalline calcium carbonate modifications [9] and is used as a transient reservoir for calcium carbonate because of its high solubility [7, 8, 10, 11].

For a better understanding of the function of the various mineral phases, information about their chemical nature and their spatial distribution would be essential. Recent studies have shown that confocal Raman spectroscopy allows the allocation of different organic compounds and the differentiation between various calcium carbonate polymorphs including ACC [12]. Nevertheless, the current work on the micro-characterization of the material is limited to structural studies mostly of de-mineralized cuticle or elemental analysis that does not allow the differentiation between ACC and calcite or the spatial allocation of different components. Combining in one instrument confocal Raman microscopy and Atomic Force Microscopy (AFM) overcomes these limitations. This combination allows the user, by simply turning the microscope turret, to link the chemical information obtained by confocal Raman microscopy with the ultra-high spatial and topographical information acquired by AFM. We imaged the structure of the sternal deposits and the dorsal cuticle of

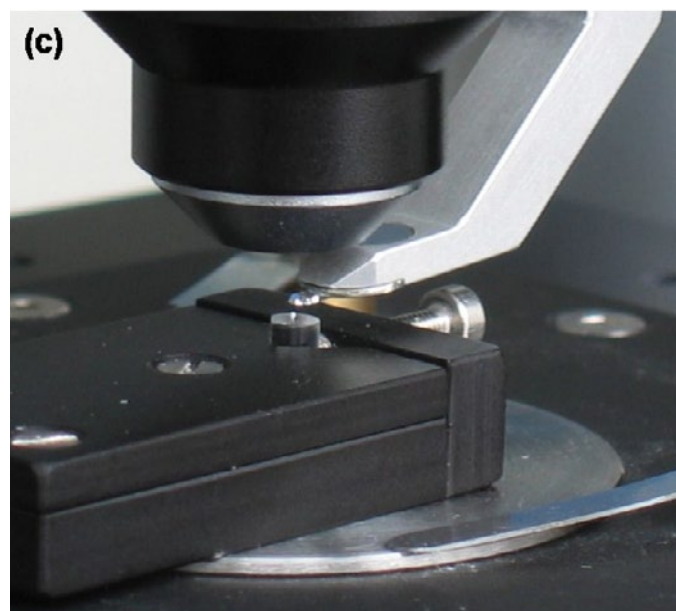
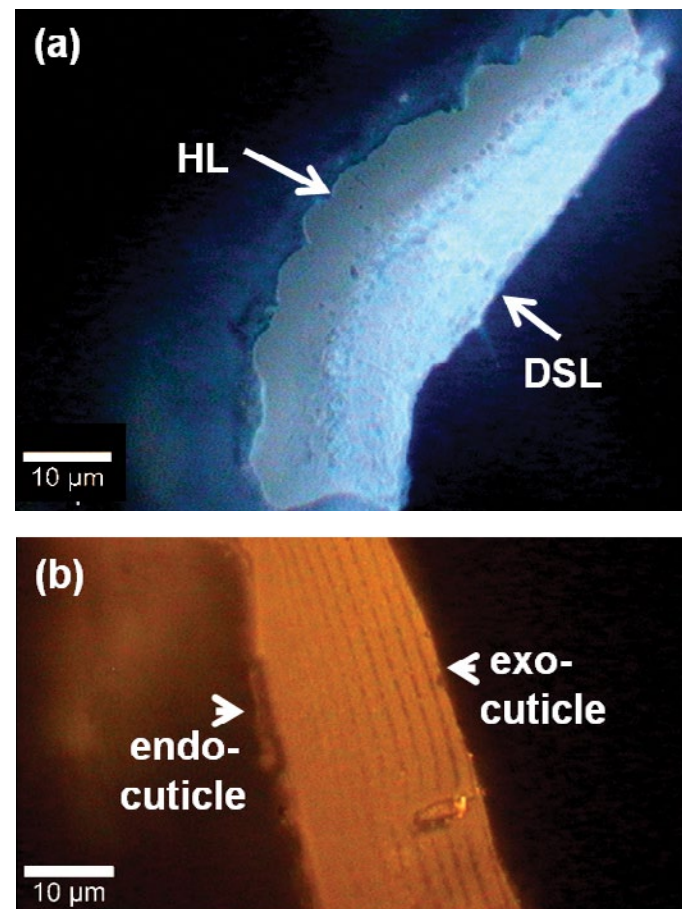
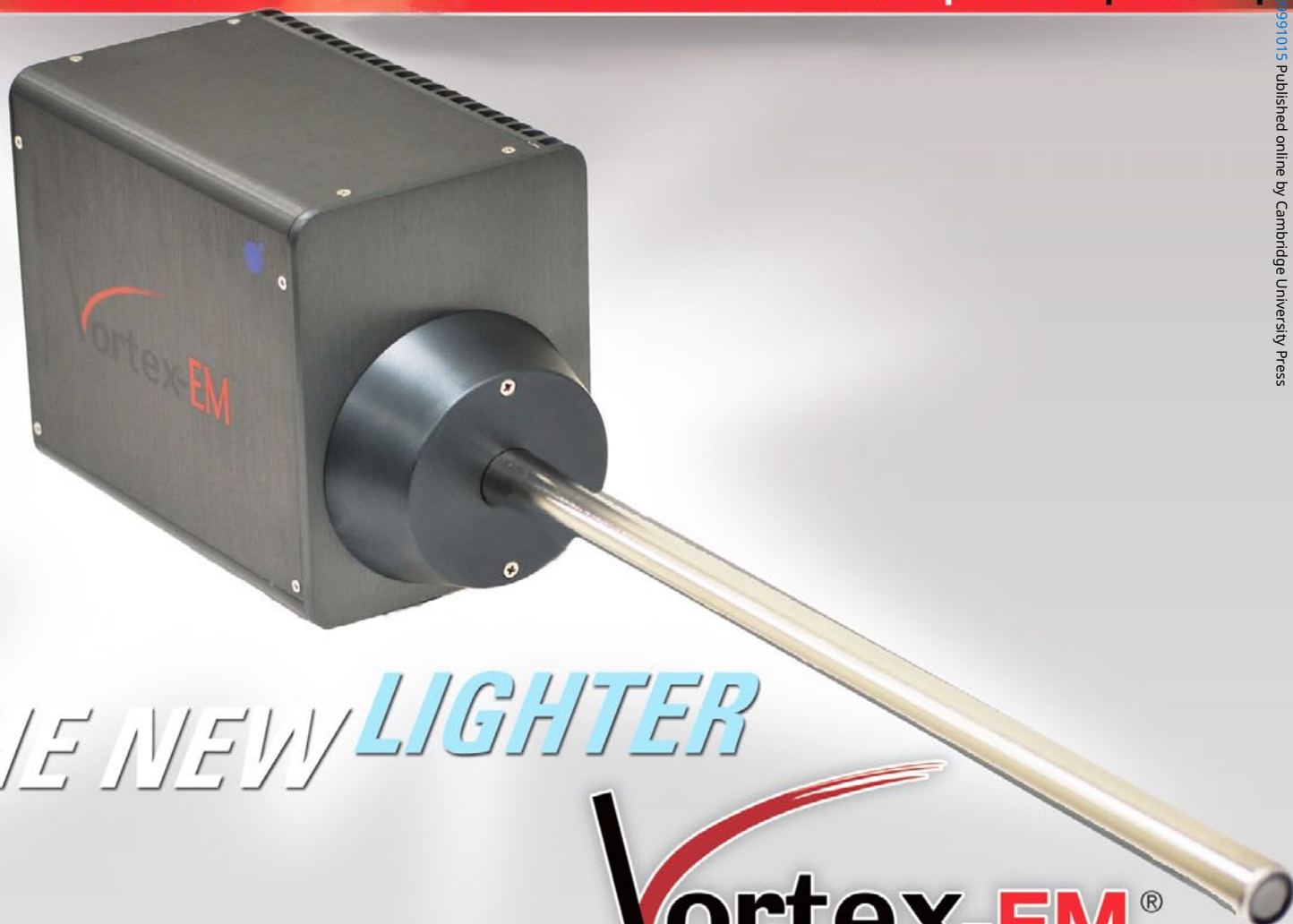


Figure 1: Video image of a knife-polished sternal deposit (a) and cuticle (b) and photograph of the alpha300 RA sample stage with the sample glued on the PMMA support and fixed in the vice (c).

NO LN2 • Active area ~ 30 mm² • <130 eV FWHM at 5.9 keV • ICR 1.5 Mcps • OCR up to 600 kcps

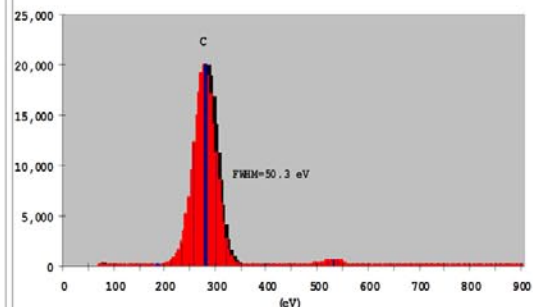
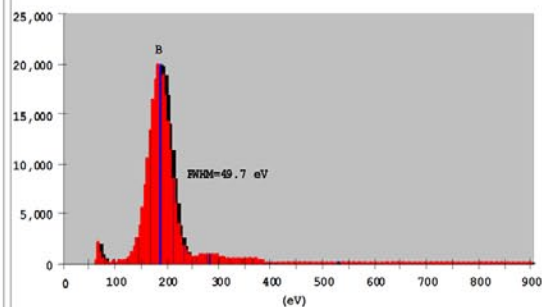
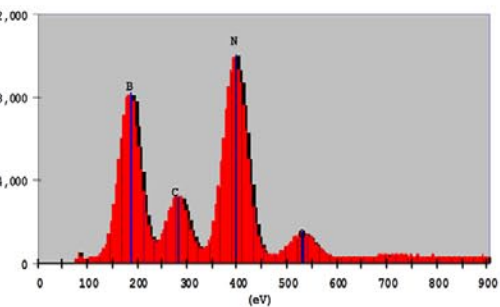


THE NEW LIGHTER

Vortex-EM®

BREAKTHROUGH PERFORMANCE

C and the B peaks are completely separated from noise by the Vortex-EM detector. It therefore, facilitates light element detection while performing microanalysis and fast elemental mapping applications.



EDS • Fast Mapping • SEM • Microanalysis • Process Control • Synchrotron • TXRF • SR-TXRF

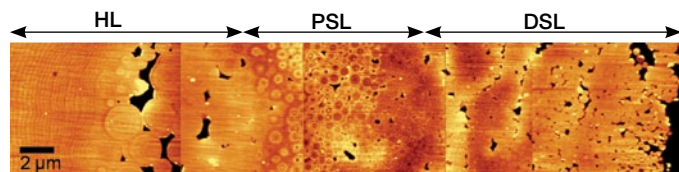


Figure 2: AFM topography overview image of a fully developed sternal deposit of *P. scaber*. ($z_{\text{max}} = 20 \text{ nm}$)

P. scaber using AFM and determined the spatial distribution of the organic and the mineral phases by confocal Raman microscopy.

Experimental Setup

Small pieces of air-dried samples of the cuticle and the sternal deposits of *P. scaber* were glued onto polymethylmetacrylate (PMMA) holders using superglue and cut sagittally using an ultramicrotome (Reichert Ultracut, Germany) with glass knives to obtain a planar surface. This surface was then polished with a diamond knife (Figures 1a and 1b). The PMMA support was then fixed in a small vice and placed on the sample stage of an alpha300 RA microscope (www.witec.de). Video images of the knife-polished specimens recorded with the eyepiece camera of the alpha300RA are shown in Figures 1a and 1b, whereas Figure 1c shows a photograph of the experimental setup. AFM measurements were performed in AC mode using an Arrow FM cantilever with a nominal spring constant of 2.8 N/m and a resonance frequency of 75 kHz (www.nanoworld.com). By simply turning the microscope turret, the alpha300 RA was transformed into a confocal Raman microscope (WITec, Ulm, Germany) equipped with a frequency doubled NdYAG laser (wavelength of 532 nm) for excitation and a Nikon 100x (NA = 0.95) air objective for imaging.

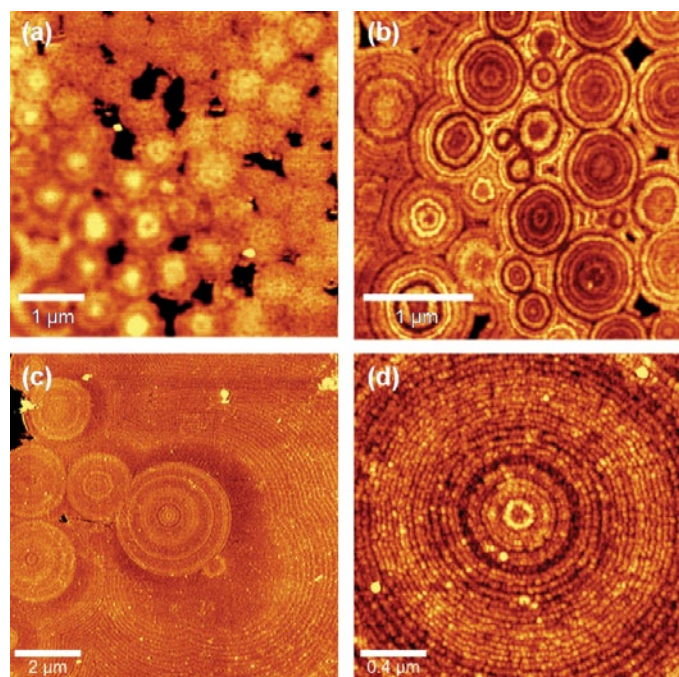


Figure 3: High-resolution AFM topography images from the DSL (a), PSL (b), and HL (c). The image (d) shows the topography of a large spherule from the transition region between HL and PSL.

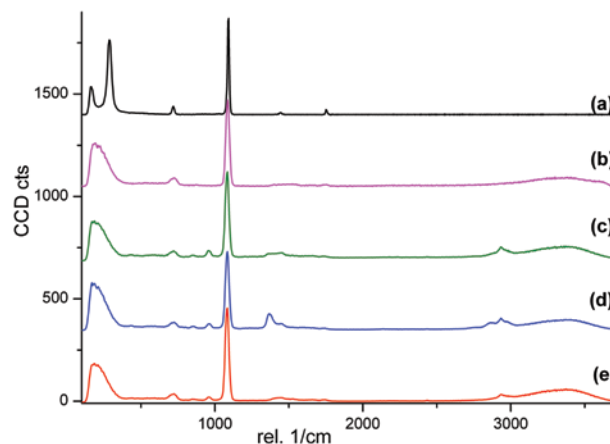


Figure 4: Raman spectra of synthetic calcite (a) and ACC (b). The following spectra show that organic molecules stabilize the amorphous CaCO_3 (ACC) of the DSL (c), PSL (d), and HL (e).

Plain calcite and ACC were synthesised as described in a previous publication [13] to obtain reference samples for most common CaCO_3 minerals. Purified chitin from crab-cuticle (Sigma-Aldrich, VWR International) served as chitin standard. The Raman spectra of the standards were recorded with integration times of 250 ms. In the Raman spectral imaging mode a complete Raman spectrum is acquired at every pixel leading to a 2D array of Raman spectra. By evaluating specific spectral features such as peak position and peak intensity, Raman images can be calculated that represent the distribution of a specific chemical compound on the surface. Furthermore, unique Raman spectra from reference materials can be used as basis spectra for the basis analysis software tool of the WITec Project software [14].

Results and Discussion

An AFM topography image of a fully developed sternal deposit from *P. scaber* can be obtained by stitching five consecutive recorded AFM images next to each other (Figure 2). The resulting chart reveals a smooth surface with an average roughness below 10 nm after the microtome polishing process. The different regions of the deposit can be clearly discriminated. The homogeneous layer (HL), which appears glassy in the light optical image (see Figure 1a), looks straticulate in the AFM image with a periodicity below 50 nm (Figure 2). The opaque regions (Figure 1a) of the deposit are composed of numerous spherules. Two layers, the proximal (PSL) and the distal spherular layer (DSL) can be distinguished (Figure 2). High-resolution AFM images reveal DSL spherules with diameters of about 500 nm, which are fused to one another (Figure 3a). The PSL spherules increase in size from distal to proximal. The spherules appear free and fuse in the transition zone towards HL. At high resolution (Figure 3b), it becomes obvious that the spherular structures consist of concentric shells composed of about 20-nm thick granules that correspond to individual ACC granules, as described by Fabritius et al. [15]. The periodic distance between the shells of the onion-like structure is less than 25 nm (Figure 3b). The spherular organization of the PSL and DSL provide a large surface for the

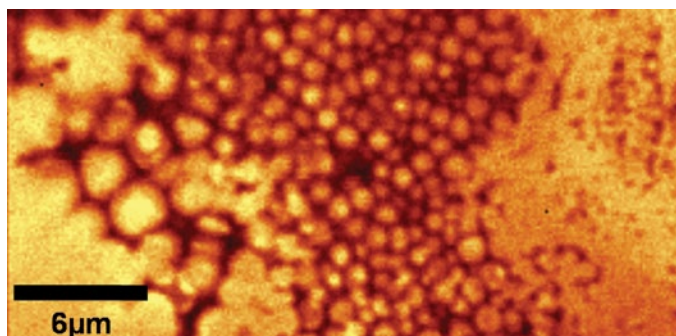


Figure 5: Distribution of amorphous CaCO_3 within the sternal deposit.

CaCO_3 deposits, which should also facilitate mobilization of calcium and carbonate ions during resorption of the deposits [16].

In the transition zone between HL and PSL, the spherules of the PSL merge. Proximally to this zone, the deposits grow into flat, stacked layers forming a stratified structure [15]. In the particular sample shown in Figure 2 and Figure 3c, spherules within the transition zone were growing unusually large. Here the AFM images nicely demonstrate the growing process of the spherules and reveal the granular substructure of the individual concentric shells (Figure 3d).

The first step to analyze the chemical composition of the deposits was to record single Raman spectra in the different layers and to compare the recorded spectra with Raman spectra of calcite and ACC standards, respectively (Figure 4). Spectra obtained from CaCO_3 (Figure 4a and 4b) show a strong Raman band in the range 1080-1090 cm^{-1} , assigned to carbonate stretching vibrations. Calcite and ACC can be discriminated because the highest intensity of this band is at 1086 cm^{-1} and 1080 cm^{-1} , respectively. For calcite distinct bands at 154 cm^{-1}

and 280 cm^{-1} , arising from lattice vibrations in the trigonal symmetry of the crystal can be detected as shown in Figure 4a [17]. These two bands broaden to one single band ranging from 100-300 cm^{-1} in the disordered ACC phase (Figure 4b) [18]. The broad band ranging from 3100-3700 cm^{-1} appearing in the ACC spectra can be assigned to the O-H stretching vibrations of the H_2O molecule [12]. This indicates that significant amounts of water are incorporated in the ACC. These differences in the spectra allow unequivocal discrimination between the two polymorphs of CaCO_3 . Single Raman spectra recorded in DSL, PSL, and HL (Figure 4c-4e) all reveal a peak at 1080 cm^{-1} and broad bands ranging from 100-300 cm^{-1} and from 3100-3700 cm^{-1} . Thus, CaCO_3 in its amorphous phase is present over the entire range of the sample, in agreement with earlier results using X-ray and electron diffraction analysis [7, 8].

An area of $30 \times 15 \mu\text{m}^2$ of a microtome-polished surface of the ACC deposit was scanned in Raman spectral imaging mode by recording an array of 265×128 Raman spectra with an integration time of 0.07 s per spectrum. Integration over the most pronounced Raman band of ACC at 1080 cm^{-1} and the broad band in the spectral range of 100-300 cm^{-1} results in an intensity image of the ACC distribution in the sternal deposit (Figure 5). Water-soluble amorphous CaCO_3 is present over the entire range of the sternal deposit. The brighter color on the left side of the image indicates a higher amount of ACC within the stratulate region of HL compared to the spherular layers. This is most likely due to the more densely packed structure.

An AFM-Raman study also was performed on the tergite cuticle of a *P. scaber*. AFM imaging of sagittally cut cuticle reveals a striated morphology, which is most likely caused by the twisted plywood arrangement of individual chitin layers. Differences in the periodicity of the striations reflect variations in stacking height resulting from a 180° turn of the chitin layers [19]. Because of this, three areas can be discriminated (Figure 6a). In a region at the inner side of the cuticle, the stack height is below 500 nm and a strong change in height (Figure 6b) can be observed. The latter is most probably caused by organic material that may shrink after drying. This region can be assigned to the non-mineralized membranous layer. In the endocuticle, located adjacent to this layer, the periodicity of

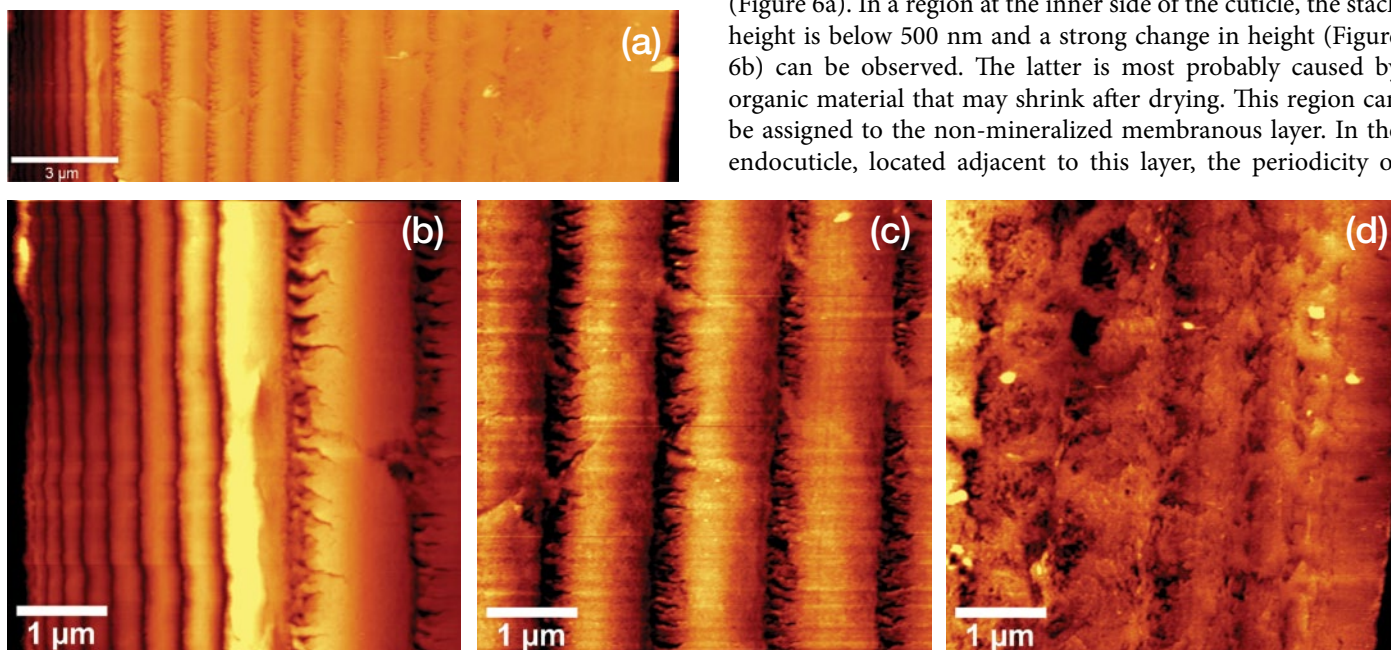


Figure 6: AFM topography overview image of the cuticle of a *P. scaber* ($z_{\text{max}} = 180 \text{ nm}$) (a) and high-resolution AFM images from the exocuticle ($z_{\text{max}} = 20 \text{ nm}$) (b), endocuticle ($z_{\text{max}} = 25 \text{ nm}$) (c), and the membranous layer ($z_{\text{max}} = 160 \text{ nm}$) (d).

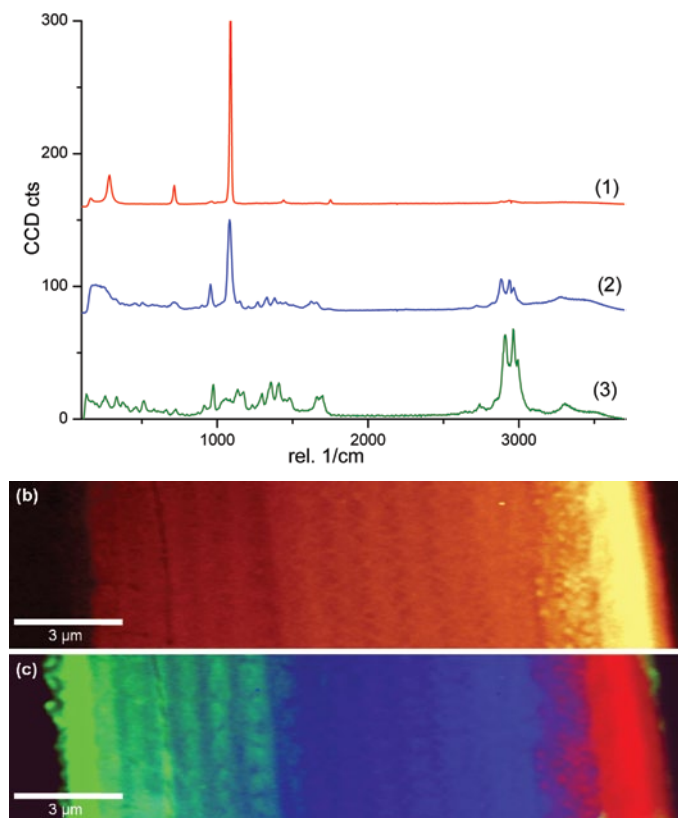


Figure 7: Raman spectra (a) evaluated from the Raman image acquired on the cuticle of a *P. scaber*. Spectrum 1 is recorded from the exocuticle and spectrum 2 from the endocuticle. Spectrum 3 is taken from the membranous layer. The image (c) shows distribution of CaCO_3 within the cuticle (b) and color-coded Raman image of the cuticle.

striation increases up to $1\ \mu\text{m}$ and the variations in height are below $25\ \text{nm}$ (Figure 6a). In an image taken at higher resolution (Figure 6c) the ripples appear smooth on top, but one can see in between the ripples fibril-like structures that are less than $100\ \text{nm}$ thick. The exterior fifth of the cuticle, which can be assigned to the exocuticle, appears flat in the overview (Figure 6a). A higher-resolution image (Figure 6d) reveals stacks, which are less ordered than in the endocuticle. Close to the surface a smooth layer can be seen, corresponding to a calcite-containing layer close to the surface (Figure 6d) [13].

To analyze the chemical composition of the cuticle, an area of $25 \times 10\ \mu\text{m}^2$ was investigated in Raman imaging mode by recording 250×100 Raman spectra with an integration time of $0.07\ \text{s}$ per spectrum. In a first step, average spectra of the exocuticle and endocuticle, as well as of the membranous layer, were generated. As shown in Figure 7a, calcium carbonate in combination with an organic matrix occurs within both exocuticle and endocuticle, but the presence of calcite is limited within the exocuticle. The membranous layer appears to be virtually devoid of calcium carbonate representing the non-mineralized organic matrix. The averaged spectra calculated from this region reveals a band with the first maximum at $3275\ \text{cm}^{-1}$ specific for amid bonds and a second maximum at $3450\ \text{cm}^{-1}$ characteristic of hydrogen bonds (Figures 7a and 3) [20]. The same band also appears in spectra

obtained for the endocuticle and exocuticle (Figures 7a, 1, and 2). This confirms that chitin is also the main non-mineralized component of the organic matrix. To study the distribution of CaCO_3 , the integral over the most pronounced Raman band of CaCO_3 at $1080\ \text{cm}^{-1}$ was calculated and plotted as an intensity image (Figure 7b). Higher amounts of mineral can be found in the exocuticle. To quantify the mineral distribution, the basis analysis procedure has been used. The spectra for pure calcite and ACC (Figures 4a and 4b) as well as the one for the organic matrix (Figures 7a and 3) were used as base spectra for the basis analysis procedure of the WITec Project software. In this procedure, each measured spectrum of the 2-D spectral array was fitted by a linear combination of basis spectra S_k using the least squares method [14]. The resulting weight factor is proportional to the quantity of the specific material and can be displayed as intensity in the corresponding Raman image such that a high value is shown in brighter color. Figure 7c shows the color-coded Raman image of the cuticle after overlaying the resulting images of calcite (red), ACC (blue), and the organic matrix (green). The Raman image confirms that calcium carbonate occurs within the whole exocuticle and endocuticle (Figure 7b). In the color-coded Raman image the two polymorphs of CaCO_3 can be unequivocally separated. Calcite is restricted to the exterior fifth of the cuticle, which corresponds to the exocuticle. In contrast to this, ACC is present within the whole endocuticle and also to a smaller extent in the inner region of the exocuticle. Towards inner regions of the endocuticle the amount of mineral decreases, and the organic matrix becomes more abundant. Within the membranous layer no stabilizing mineral can be found. Therefore, this region can shrink to a higher extent than the endocuticle and appears smaller in the AFM images (Figures 6a and 6b).

Conclusions

The combination of AFM and confocal Raman microscopy in a single instrument allows the nondestructive characterization of heterogeneous biological materials. In combination with a powerful software package, chemical identification of small sample volumes becomes available at very short integration times per spectrum. It could be shown that the mineral phase within the sternal deposits of the *P. scaber* consists of the amorphous phase of CaCO_3 . High-resolution AFM images revealed the presence of a three-layered structure. The spherular organization of two of these layers provides a large surface of CaCO_3 deposits, facilitating the mobilization of calcium and carbonate ions during resorption of the deposit.

In the cuticle of *P. scaber*, two polymorphs of CaCO_3 were detected next to each other by Raman imaging. The protective calcite phase is present only in the exocuticle, whereas the amorphous ACC phase is present within the whole endocuticle. Structural changes observed with the AFM while imaging the cuticle can be linked with the chemical composition from Raman imaging, thus leading to the correlation between chemical composition and the constructional morphology of the cuticle. **MT**

References

- [1] Y Bouligand, *Tissue Cell* 4 (1972) 189-217.
- [2] G Luquet and F Marin, *Comptes Rendus Palevol* 3 (2004) 515-534.
- [3] A Ziegler et al., *Micron* 36 (2005) 137-153.
- [4] A Becker et al., *Dalton Transactions* (2005) 1814-1820.
- [5] F Neues et al., *Crystal Engineer Community* 9 (2007) 1245-1251.
- [6] A Ziegler and B Miller, *Zoomorphology* 117 (1997) 181-187.
- [7] A Becker et al., *Dalton Transactions* (2003) 551-555.
- [8] A Ziegler, *J Struct Biol* 112 (1994) 110-116.
- [9] E Beniash et al. *P Roy Soc Lond B Bio* 264 (1997) 461-465.
- [10] L Brecevic and AE Nielson, *J Cryst Growth* 98 (1989) 504-510.
- [11] S Raz e al., *Biol Bull* 203 (2002) 269-274.
- [12] J Aizenberg et al., *J Am Chem Soc* 124 (2002) 32-39.
- [13] S Hild et al., *J Struct Biol* 163 (2008) 100-108.
- [14] U Schmidt et al., *Macromol Symposia* 230 (2005) 133.
- [15] H Fabritius et al., *J Struct Biol* 150 (2005) 190-199.
- [16] H Fabritius and A Ziegler, *J Struct Biol* 142 (2003) 281-291.
- [17] H N Rutt and J H Nicola, *J Physiology C* 7 (1974) 4522-4528.
- [18] M M Tlili et al., *J Raman Spectrosc* 33 (2001) 10-16.

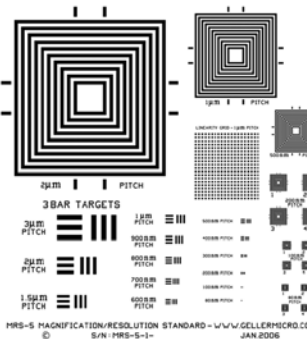
MRS-5

We are ISO-9000 certified and ISO-17025 accredited

Microscopy Calibration Standard


Now you can calibrate from 1,000X to 1,000,000X!

This is our fourth generation, traceable, magnification reference standard for all types (SEM, FESEM, Optical, STM, AFM, etc.) of microscopy. The MRS-5 has multiple X and Y pitch patterns ranging from 80nm (±1nm) to 2µm and 3 bar targets from 80nm to 3µm. There is also a STM test pattern.



MRS-5 MAGNIFICATION/RESOLUTION STANDARD - WWW.GELLERMICRO.COM
© GELLER MICROANALYTICAL LABORATORY, INC. JAN 2006

Free web resource guide!




**GELLER
MICROANALYTICAL
LABORATORY, Inc.**

426e Boston St., Topsfield, Ma 01983
www.gellermicro.com

Did You KNOW?

Evactron® De-Contaminators can EASILY and AFFORDABLY be added to your EXISTING TEM, SEM or FIB.

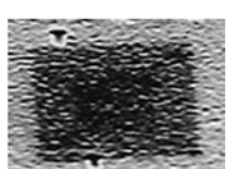


WHY is this IMPORTANT?

To get the BEST IMAGES possible, by improving resolution and contrast.

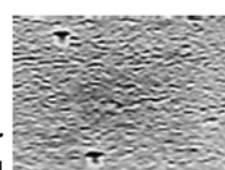
HOW does it work?

The Evactron D-C removes carbon from vacuum systems with oxygen radicals.



Before

Gets rid of contamination artifacts.



After Cleaning

Bottom Line

More Info? Visit or Call:

XEI SCIENTIFIC, INC.

1755 East Bayshore Rd, Suite 17, Redwood City, CA 94063
(650) 369-0133, FAX (650) 363-1659
email: sales@Evactron.com

www.EVACTRON.COM